UC Merced
UC Merced Previously Published Works

Title

Thermal decomposition of phosphonium salicylate and phosphonium benzoate ionic liquids

Permalink

https://escholarship.org/uc/item/2zn3b33c

Authors

Khajeh, Arash
Rahman, Hafizur
Liu, Ting
et al.

Publication Date

2022-04-01

DOI

10.1016/j.molliq.2022.118700

Peer reviewed

Thermal decomposition of phosphonium salicylate and phosphonium benzoate ionic liquids

Arash Khajeh,[†] Md Hafizur Rahman,[‡] Ting Liu,[†] Pawan Panwar,[†] Pradeep L. Menezes,[‡] and Ashlie Martini[*,†]

[†]Department of Mechanical Engineering, University of California Merced, CA 95343, USA

[‡]Department of Mechanical Engineering, University of Nevada-Reno, Reno, NV 89557, USA

E-mail: amartini(at)ucmerced.edu

1

Abstract

The thermal stability of ionic liquids is important for their use in a variety of applications. Here, reactive molecular dynamics simulations and thermogravimetric analysis were used to explore the thermal decomposition mechanisms of phosphonium salicylate and phosphonium benzoate. Experiments performed at different heating rates indicated that the decomposition temperatures of phosphonium salicylate and phosphonium benzoate were comparable, but phosphonium benzoate was less stable than phosphonium salicylate under isothermal high temperature conditions. The lower thermal stability of the benzoate compared to the salicylate was reproduced in reactive molecular dynamics simulations. The simulations also showed that cation chain length had little effect on thermal stability. The simulations revealed that thermal decomposition for both phosphonium salicylate and phosphonium benzoate occurred through many different pathways that could be broadly categorized as proton-transfer, association, and dissociation reactions. The phosphonium benzoate underwent more of these reactions and exhibited a wide range of reaction pathways in each category than the phosphonium salicylate. Multiple possible mechanisms were explored to explain this difference and it was found that the dominant factor was the presence of the hydroxyl group in salicylate that affects the ability of oxygen atoms to take part in proton-transfer reactions that are the first step of all subsequent reactions. These findings demonstrate that even subtle differences in anion chemistry may significantly affect the thermal stability of ionic liquids, suggesting avenues for tuning these properties through molecular design.

Introduction

Ionic liquids (ILs) are low-melting temperature molten salts composed of anions and cations, and many of them are in liquid state at room temperature.[1,2] They have unique properties including low vapor pressure,[3,4] high ionic conductivity,[5,6] high thermal stability,[7,8] and the ability to dissolve a variety of chemical compounds.[9,10] This combination of properties make

2

ILs suitable candidates for a range of applications such as solvents,[11,12] display screens,[13,14] fuel cells,[15,16] battery electrolytes,[17,18] gas separation membranes,[19,20] and lubricants.[21,22] For ILs to function effectively in many of these applications, they must withstand high temperatures (usually above 373 K)[23–26] Thus, the thermal stability of ILs is of great importance and has been the subject of many studies over the last few decades.[27–35]

There are several classes of ILs including imidazolium, pyridinium, ammonium, phosphonium, and sulfonium.[36] Among these, phosphonium ILs are particularly important because they are relatively inexpensive, and already applied in some industrial processes.[37–39] Phosphonium ILs also have very good thermal stability. However, the thermal stability is not the same for all phosphonium ILs since the cation can have different length alkyl chains and side chains and be paired with various anion structures.[40–42] Although the size and structure of the phosphonium cation can vary, several previous studies[42,43] suggested that the anion plays a more significant role in thermal stability than the cation. These studies associated the degradation pathway mainly to the anion. Some previous studies[43,44] attributed the prominent role of the anion to the steric hindrance applied by the alkyl chains to the positively charged phosphorus in the phosphonium, which interferes with the electrostatic interactions between the anion and the cation.

Several experimental studies explored the thermal stability of phosphonium-based ILs with different anion structures.[42,45,46] Such studies employed various experimental methods including thermogravimetric analysis (TGA),[46] gas chromatography-mass spectroscopy (GC-MS),[47] thermogravimetric-mass spectrometry (TG-MS),[48] pyrolysis gas chromatography (PyGC),[49] thermal desorption-mass spectroscopy (TD-MS),[50] Fourier transform infrared spectroscopy (FTIR),[51,52] and time-of-flight mass spectrometry (TOF-MS).[53] These techniques were used to explore parameters such as decomposition temperature,[46] decomposition products,[47,50] and evolution of chemical structure during the heating.[51–53]

Atomistic simulations, both ab initio and classical molecular dynamics (MD), have been employed to study the thermal decomposition of phosphonium-based ILs.[54] These methods

3

were used to investigate various parameters and phenomena, including interactions between anions and cations, spatial distribution functions, reaction pathways, energy barriers for decomposition reactions, decomposition products, and reaction mechanisms.[52,55,56] Previous studies have suggested that high nucleophilicity[45,52,55] and basicity[45,57] of anions affects the thermal stability of phosphonium-based ILs. However, previous studies used either density functional theory (DFT) calculations, which can not model the complex interactions between many anions and cations in large model systems over long durations, or classical MD simulations, which do not model the chemical reactions that are necessarily part of thermal decomposition.

An alternative simulation approach is reactive MD that can capture chemical reactions in relatively large model systems.[58,59] Among reactive MD force fields, ReaxFF[60] has been developed for a wide range of materials and processes. ReaxFF MD simulations have been used to investigate thermal decomposition of various chemical species, including polymers,[61] hydrocarbon fuels,[62–64] refrigerants,[65,66] insulation gas,[67] energetic materials,[68,69] and phosphate-based lubricant additives.[70,71] For ILs specifically, ReaxFF MD simulations have been used to study interactions between ILs and carbon dioxide for gas separation applications,[72] hypergolicity,[73] and electrolyte reduction pathways.[74] One study used hybrid DFT-ReaxFF simulations to model degradation reduction reactions of lithium bis-(trifluoromethanesulfonyl)imide, but the reactions occurred at room temperature.[75] There have been no reactive MD-based studies of the high temperature stability of ILs.

The above review shows the importance of anion structure in the thermal stability of ILs. However, to understand how the anion affects thermal decomposition, particularly of phosphonium-based ILs, atomistic simulations are required. Therefore, in this study, we combined TGA experiments and ReaxFF MD simulations to characterize the thermal decomposition of phosphonium salicylate and phosphonium benzoate. The similar chemistries of these ILs enabled isolation of the effect of the anion such that the origin of differences in thermal stability observed in the experiments could be explained using the atomistic detail

4

available in the reactive MD simulations.

Methods

Experiments

To quantify thermal stability, thermogravimetric analyses (TGA) were performed with two phosponium ILs, $[P_{6,6,6,14}]$ salicylate and $[P_{6,6,6,14}]$ benzoate, synthesized from an ion exchange reaction using $[P_{6,6,6,14}]$ and sodium salicylate, or sodium benzoate, as described earlier by Egorov et al.[76,77] TGA experiments were performed using a Shimadzu TGA 50 thermogravimetric analyzer in two phases. First, thermogravimetric degradation was performed at a heating rate of 10 K/min up to 1073 K (800 °C), following ASTM E 2550-17[78] standard. An argon flow rate of 20 ml/min was used throughout the experiment to ensure an inert atmosphere. Tests were also carried out at heating rates of 20 and 40 K/min for both ILs. In the second phase, isothermal decomposition was studied for both ILs. Wooster et al.[79] established a methodology to predict the maximum operable temperature for IL-based lubricants. In this method, lubricants were isothermally heated for 10 hours at a given temperature and the lubricant was considered operable at that temperature if less than 1% decomposition occurred. This method has been used to characterize IL lubricants by other researchers.[80,81] Here, to assess the thermal stability of phosphonium salicylate and phosphonium benzoate, isothermal thermogravimetric analyses were performed in an argon atmosphere at 373 K (100 °C), and 423 K (150 °C), set points. A heating rate of 20 K/min was used to reach the isothermal setpoint, followed by 10 hours of isothermal heating.

Reactive Molecular Dynamics Simulations

Reactive molecular dynamics (MD) simulations of phosphonium salicylate and phosphonium benzoate were performed using a ReaxFF force field originally developed for modeling the interactions between phosphonium glycinate and CO_2.[72] To avoid the excessively close range

non-bonded interactions, a shielding term was used in all simulations, as suggested in a previous study.[72] The model systems comprised 100 cations and 100 anions in a periodic simulation box with side lengths of 12 nm. The effect of cation and anion was studied by modeling phosphonium cations of three different sizes of $[P_{4,4,4,4}]^+$, $[P_{4,4,4,8}]^+$, or $[P_{6,6,6,14}]^+$ and either salicylate or benzoate anions, shown in Fig. 1. Although a small amount of water was likely present in the synthesized phosphonium ILs,[82–84] water was not included in the models.

Each system was equilibrated with an isothermal–isobaric (NPT) ensemble (constant number of atoms N, pressure P, and temperature T) for 3 ns. The time step during equilibration was 0.5 fs, and the temperature was maintained at 300 K using a Nosé-Hoover thermostat[85] with a temperature damping parameter of 50 fs while the pressure was maintained at 1 atm using a Nosé-Hoover barostat and a damping parameter of 500 fs. The equilibration was continued until steady density and potential energy were reached. Next, to capture the bond formation and bond breaking phenomena accurately, the time step was decreased to 0.25 fs, and the damping parameter for the thermostat and barostat changed to 25 and 250, respectively. Then equilibration at 300 K and 1 atm was continued for another 200 ps to ensure that decrease in the time step did not affect the equilibration. Finally, the temperature was ramped to 900 K at a rate of 1 K/ps with the same time step and damping parameters as used in the second equilibration step.

The connectivity of atoms obtained from the ReaxFF bond table was post-processed using user-defined python scripts to identify the reactants, intermediate species, and products of the chemical reactions. A bond order cutoff of 0.5 was used to identify the bonding within each chemical species. The bond order cutoff was the same for all possible atom pairs. The weight percentage of unreacted ILs was quantified based on the change in the number of chemical species whose molecular weight corresponds to the original cations and anions. All molecular dynamics simulations were performed using a large-scale atomic/molecular massively parallel simulator (LAMMPS)[86] MD package, and the results were visualized
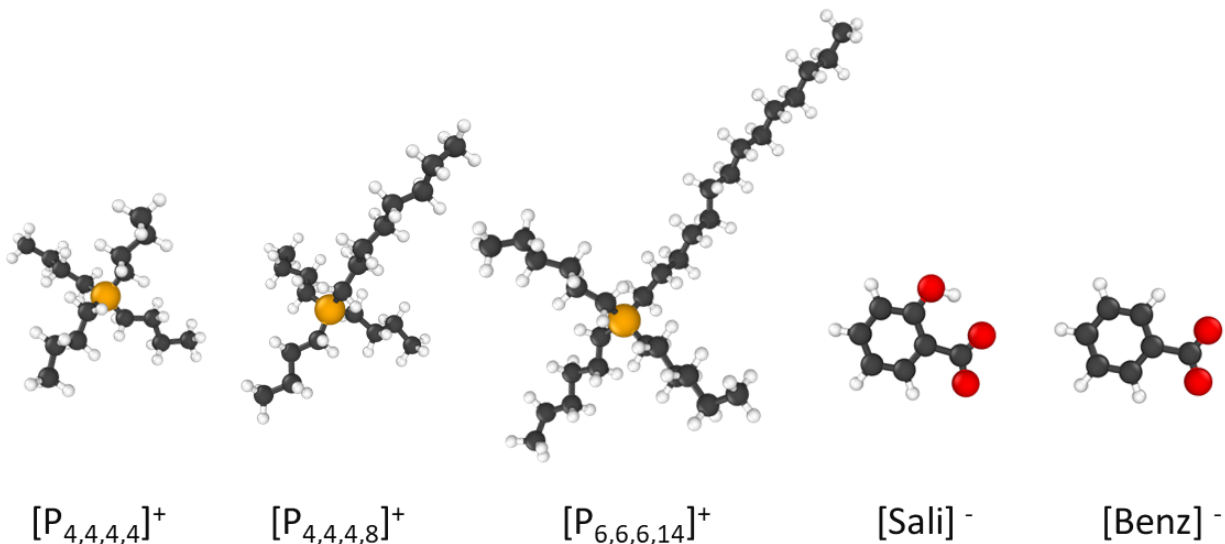
Figure 1: IL systems studied in this research included phosphonium cations with different sizes $[P_{4,4,4,4}]^+$, $[P_{4,4,4,8}]^+$, or $[P_{6,6,6,14}]^+$ paired with salicylate ($[Sali]^-$) or benzoate ($[Benz]^-$) anions. White, dark gray, red and orange spheres represent hydrogen, carbon, oxygen, and phosphorous elements, respectively.

Results

Themogravimetric Experiments

To evaluate the thermal stability of phosphonium-based ILs, TGA experiments were performed on phosphonium salicylate and phosphonium benzoate by heating from room temperature to 900 K at 10, 20, and 40 K/min heating rates. As shown in Fig. 2, the thermal decomposition of $[P_{6,6,6,14}]$ salicylate and $[P_{6,6,6,14}]$ benzoate did not start until around 475 K. The decomposition temperature (T_d) was calculated for each IL per the ISO 11358-1[88] standard as the intercept of a linear fit to the steepest part of wt% vs temperature graph and the horizontal line passing through 100% wt. At a heating rate of 10 K/min, the decomposition temperature was 623 K and 628 K for phosphonium salicylate (Fig. 2(a)) and phosphonium benzoate (Fig. 2(b)), respectively. This indicates that the both phosphonium-based

7

ILs studied here have high thermal stability making them suitable for high-temperature applications. The decomposition temperature increased for both phosphonium salicylate and phosphonium benzoate with increasing heating rate. However, at any heating rate, the decomposition temperatures of the two ILs were within the 6 degree repeatability range specified by the ASTM standard,[78] indicating the difference in their thermal stability was statistically insignificant.
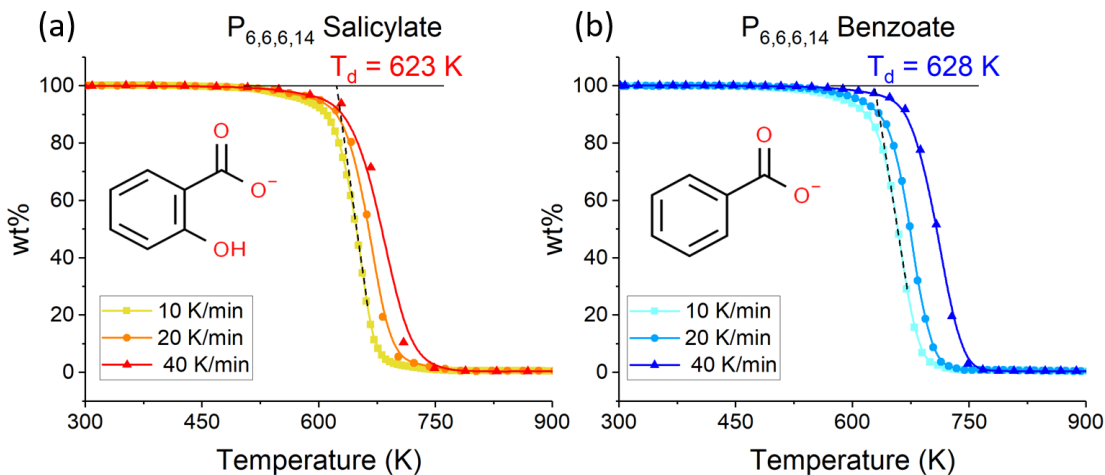

Figure 2: Thermogravimetric analysis of $[P_{6,6,6,14}]$ salicylate and $[P_{6,6,6,14}]$ benzoate at different heating rates.

The results from the isothermal TGA tests are shown in Fig. 3. It can be observed that both salicylate and benzoate-based ILs exhibited less than 1% decomposition over 10 hours duration at 373 K. However, the decomposition of benzoate (99.3%) was slightly more than that of salicylate (99.8%). This difference was more prominent when the isothermal heating was carried out at 423 K (92.0% for benzoate and 98.7% for salicylate). This observation indicates that phosphonium benzoate is thermally less stable compared to phosphonium salicylate at high temperatures. A similar trend of thermal stability was observed previously.[77] In our current investigation, the atomic mechanisms underlying this difference were studied using reactive MD simulations.

The thermal decomposition results from MD simulations are shown in Fig. 4. In the
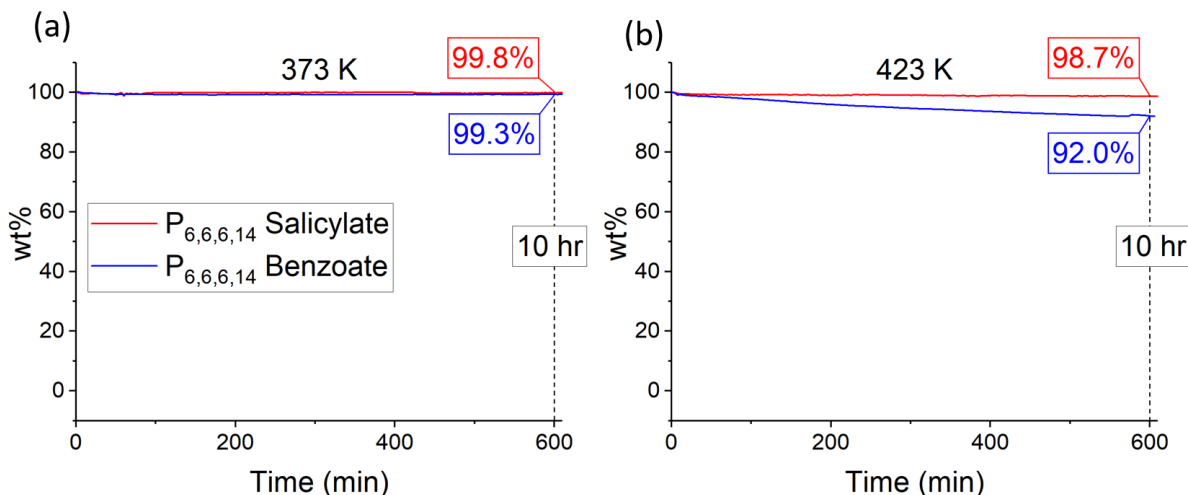
Figure 3: Thermal decomposition of $[P_{6,6,6,14}]$ salicylate and $[P_{6,6,6,14}]$ benzoate for 10 hours of isothermal heating.

162 simulations, decomposition was quantified as percent of chemical species having chemical
163 compositions equal to that of the original anions and cations (called unreacted ILs). The
164 decomposition temperature T_d was calculated by first fitting a sigmoid function to the wt%
165 of unreacted ILs and then finding the intersection between the line tangent to the steepest
166 part of this sigmoid graph and the horizontal line passing through 100% wt. As shown in
167 Fig. 4, the average value for the onset of thermal decomposition temperature of phospho-
168 nium salicylate with three phosphonium sizes was significantly higher (668 K) compared to
169 benzoate (486 K). This is consistent with the trends observed from the isothermal TGA
170 results in Fig. 3.

171   The simulations also enabled characterization of the effect of the cation size on thermal
172 decomposition. Simulations of ILs with $[P_{4,4,4,4}]^+$, $[P_{4,4,4,8}]^+$, and $[P_{6,6,6,14}]^+$ showed that
173 $[P_{6,6,6,14}]^+$ had the highest decomposition temperature (693 K for salicylate and 494 K for
174 benzoate) compared to $[P_{4,4,4,4}]^+$ (673 K for salicylate and 476 K for benzoate) and $[P_{4,4,4,8}]^+$
175 (637 K for salicylate and 488 K for benzoate). The statistical error associated with the sim-
176 ulation results was evaluated by performing repeat simulations for $[P_{4,4,4,8}]^+$ and $[P_{6,6,6,14}]^+$
177 benzoate. It was found that the average standard error in the calculated decomposition tem-

perature was 17.5 K. Since the difference between the decomposition temperatures of ILs with the same anion but different cation was comparable to this error, the effect of cation was assumed to be not statistically significant. We, therefore, focused on the effect of the anion.

Despite the consistent trends in experiments and simulations, it should be noted that there are several key differences between the TGA experiments and MD simulations. First, the method of quantifying thermal decomposition is different between the two studies. In the TGA experiments, the decrease in the weight occurs due to the evaporation of ions that decompose and form volatile species due to heating. However, the system in MD simulation is a closed box, and the results in Fig. 4 are based on the weight of ions that preserved their initial chemical composition. Second, the heating rate is several order of magnitude higher in simulations than in experiments, which is due to the high computational cost of the simulations. The higher heating rates are expected to increase the onset temperature for most chemically activated reactions as they require both time and energy to take place.[70,89–92]

Finally, despite the careful drying process use for the ILs before TGA, there is expected to be some amount of residual water in experiments. In contrast, the reactive MD simulations model neat ILs. To confirm that the presence of water would not affect model results, test simulations were run with $[P_{4,4,4,4}]^+$ benzoate or salicylate with 100 water molecules. Results showed that hydrogen transfer occurred between the water and anions, which affected the rate of IL decomposition, but that the trend was the same, i.e., $[P_{4,4,4,4}]^+$ salicylate was more thermally stable than the benzoate. Importantly, despite the differences between experiments and simulations, both showed the same trend of higher thermal stability of salicylate compared to benzoate, which indicates that the reactive MD simulations are a reasonable model of this material system and can be used to identify the mechanisms underlying the observed IL thermal stability.

To understand the differences in the thermal stability of phosphonium salicylate and benzoate, chemical reactions were identified through the connectivity of atoms and composition
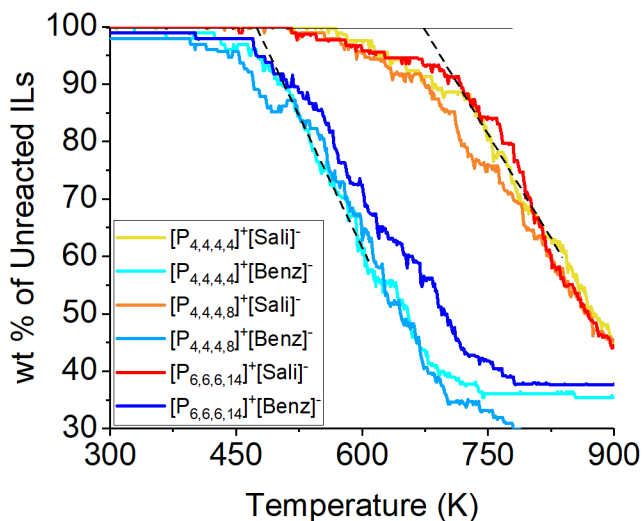
Figure 4: Weight percentage of unreacted ILs in reactive MD simulations as a function of temperature. Simulations show the onset temperature of thermal decomposition is higher for phosphonium salicylate than phosphonium benzoate, which indicates the higher thermal stability of phosphonium salicylate. The difference in the thermal decomposition temperature of ILs with the same anion but different size of cations ($[P_{4,4,4,4}]^+$, $[P_{4,4,4,8}]^+$, and $[P_{6,6,6,14}]^+$) was not statistically significant.

of chemical species. Figs. 5(a) and (b) show representative reactions in $[P_{4,4,4,4}]^+$ salicylate and $[P_{4,4,4,4}]^+$ benzoate, respectively. As can be seen in these figures, the reactions can be classified into three categories: proton-transfer, association, and dissociation reactions. In proton-transfer reactions, a positively charged hydrogen ion transfers between the phosphonium cation and benzoate/salicylate anion. In these figures, the blue spheres help readers identify the proton transferred between the cation and anion. In association reactions, the cation and anion form heavier species through covalent bonding. Finally, in dissociation reactions, covalent bond breaking results in the formation of two or more lighter fragments. As shown in Fig. 5, both phosphonium salicylate and benzoate underwent all three types of reactions.

All reactions that occurred during the temperature ramp simulations were tracked and those observed at least ten times during the simulation are reported in Fig. 6. In this figure, the labels on the vertical axis describe the chemical reactions in condensed form with the
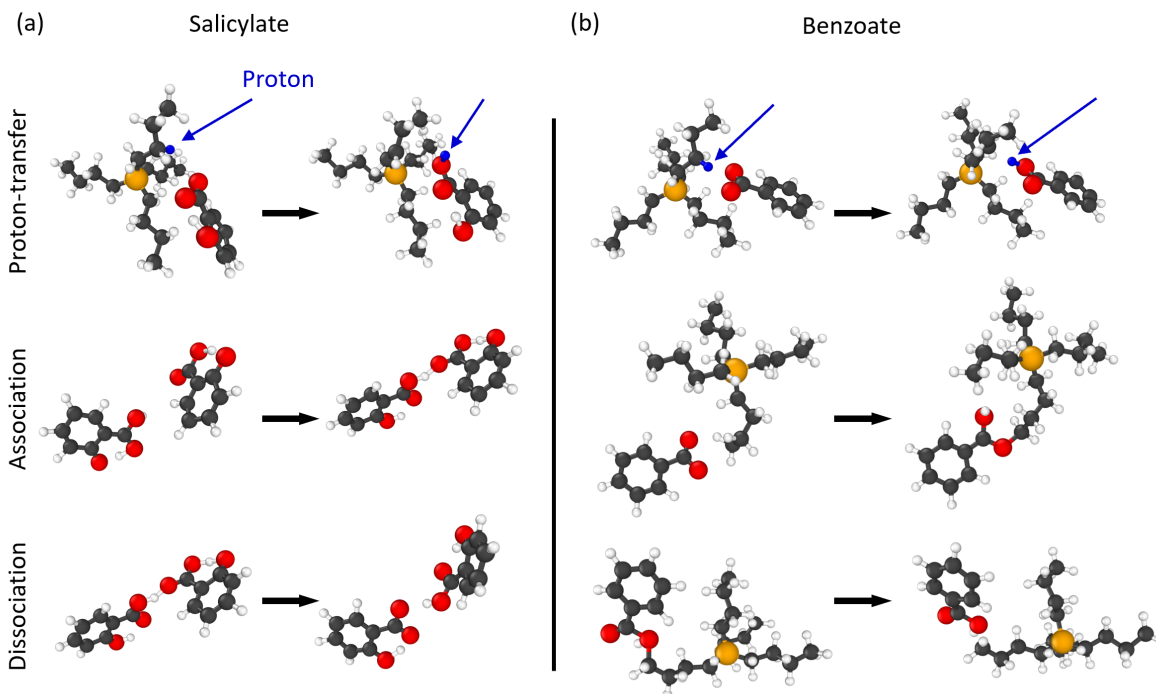
11

Figure 5: Representative reactions for (a) salicylate and (b) benzoate. The reactions can be classified into three categories: proton-transfer, association, and dissociation.

atom types ordered from heaviest to lightest followed by the number of each atom type. Each symbol corresponds to one occurrence of a chemical reaction. The data is presented in box-and-whisker plots to enable identification of the start and end temperatures for each reaction and the interquartile range in which 50% of reactions occur. The reactions are also categorized into the three main categories, proton-transfer, association, and dissociation (see the labels on the vertical axis). As shown in Fig. 6, the number of distinct chemical reactions in each category is higher for phosphonium benzoate than phosphonium salicylate. Also, more occurrences of reactions (more symbols) can be observed in the case of phosphonium benzoate compared to phosphonium salicylate. The greater number and diversity of chemical reactions is directly related to the lower thermal stability of phosphonium benzoate than phosphonium salicylate.

Previous studies attributed the reactivity of ILs primarily to the anions.[42,56,93] Further, some of these studies correlated thermal stability to the anion basicity/nucleophilicity in

12

phosphonium-based ILs[42] and other IL systems.[94,95] This correlation was investigated here using the MD simulations of phosphonium salicylate and benzoate. As can be seen in Fig. 6, the first chemical reaction (i.e., the reaction that occurred at the lowest temperature) for both ILs was the deprotonation of the phosphonium cation by the salicylate/benzoate anion. Proton-transfer reactions between the cation and anion have been previously reported in phosphonium-based ILs[96,97] and in other systems, including native-like protein ions,[98,99] hypergolic fuels ILs,[100] and amino acid[101] ILs. It was also reported that the energy barriers for proton-transfer reactions are much lower than other reactions in thermal decomposition of hydrocarbons.[64]

Once the first proton-transfer reaction happens, the newly formed species can take part in subsequent reactions as a reactant. In fact, all reactions that happen at higher temperatures involve the products of the first proton-transfer reactions (protonated anions and deprotonated cations) either directly or indirectly. This dependence is illustrated graphically in Fig. S1 for phosphonium salicylate. As shown in Fig. 6, the first proton-transfer reaction in phosphonium benzoate occurs at a significantly lower temperature (380 K) than in the phosphonium salicylate (510 K). Then, since all subsequent reactions rely on that first proton-transfer reaction, the lower thermal stability of phosphonium benzoate can be attributed to the lower onset temperature of the proton-transfer reactions. The lower onset temperature of proton-transfer for benzoate compared to salicylate observed in our simulations shows that benzoate is more basic (more capable of replacing protons from phosphonium) and, therefore, thermally less stable than the salicylate anion. These observations confirm the correlation between basicity and thermal decomposition of ILs reported in previous studies.[42,94,95]

The chemical reactions presented in Fig. 6 occur in both the forward and backward directions. To better understand these reactions, the net number of reactions (the number occurrences for each reaction in the forward direction minus the number of occurrences in the backward direction) was calculated. The most commonly observed reactions are illustrated in the snapshots in Fig. 7 and Fig. 8 for phosphonium salicylate and phosphonium
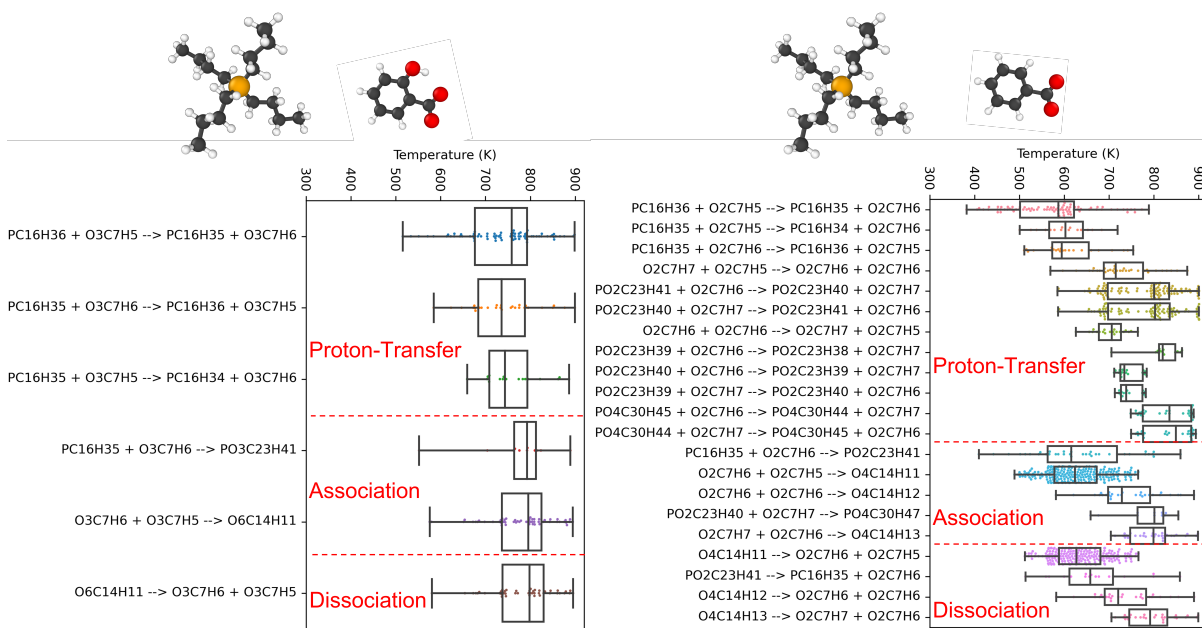
13

Figure 6: Distribution of chemical reactions detected in phosphonium salicylate and phosphonium benzoate as a function of temperature. The chemical reactions can be categorized as proton-transfer, association, or dissociation. Each symbol represents one out of at least ten occurrences of a given reaction. More chemical reactions were observed at lower temperatures for phosphonium benzoate than phosphonium salicylate, consistent with the observed lower thermal stability of phosphonium benzoate. In both systems, the proton-transfer reactions are the first step and occur at lower temperatures than the other reactions. All subsequent reactions involve the products of proton-transfer reactions.

benzoate, respectively, in order of the net number of occurrences from top to bottom. In these figures, the newly transferred proton is shown in blue, as a solid sphere on the anion and a dashed blue circle on the cation. Also, the hydrogens that were removed from the cation in previous reactions are shown as dashed red circles. The most frequent reaction in both IL systems is the proton-transfer from a phosphonium cation to an anion (see Fig. 7(a) and Fig. 8(a)). These observations again emphasize the importance of proton-transfer reactions in the thermal decomposition of both phosphonium salicylate and phosphonium benzoate. In both systems, we also observe that the three carbon atoms near the end of the alkyl chain participate in the proton-transfer reactions. The carbon atoms bonded to the phosphorous atom did not participate in such reactions, likely because of steric hindrance or difficulty of the anions to approach this carbon due to the long alkyl chains.

14

As shown in Fig. 7(b) and (c), for phosphonium salicylate, the next most frequent reactions after an initial proton-transfer are subsequent proton-transfer reactions from a cation that previously lost one or two protons to a salicylate ion. These figures illustrate that the second and third protons transfers from a carbon atom adjacent to a previously reacted carbon atom to a salicylate anion (see how blue dashed spheres are next to red dashed spheres). In contrast, in phosphonium benzoate, the next most frequent reactions after the first proton-transfer are association between anions and deprotonated cations or dissocated cations (Fig. 8 (b), (c), and (d)), followed by proton-transfer from associated species and protonated ions to benzoate anions Fig. 8 (e) and (f)). Interestingly, in Fig. 8 (c) and (d), we see some phosphonium fragments in which the phosphorus atoms are bonded to an oxygen atom. It appears the dealkylation of phosphonium involves bonding between the oxygen atom in the phosphorous in the cation; an observation made only for phosphonium benzoate.

In both Fig. 7 and Fig. 8 the unreacted phosphonium cations do not take part in any reactions except an initial proton-transfer to anions. This is opposite to the behaviour of anions, which indicates that proton-transfer from cation to anion makes the cation more reactive and the anion less reactive. This observation is confirmed by the fact that the number of cations decreases with increasing temperature more slowly than the number of anions (Fig. S2). The above observed trends are again consistent with previous studies that attributed the reactivity of ILs primarily to the anions.[42,56,93]

The difference between the thermal stability of phosphonium salicylate and phosphonium benzoate ILs is surprising given their very similar structures (see Fig. 9). Both anions form from a carboxylate group attached to a benzene ring. The salicylate has a hydroxyl group on the ring next to the carboxylate group position that is not present in the benzoate ion. As discussed before, the difference between the thermal stability of the two systems is related to their proton-transfer reactions. This suggests that the presence of hydroxyl group affects the ability of oxygen atoms to take part in the proton-transfer reactions. In other words, the protonation reaction of salicylate and benzoate ions should reflect the trend of thermal
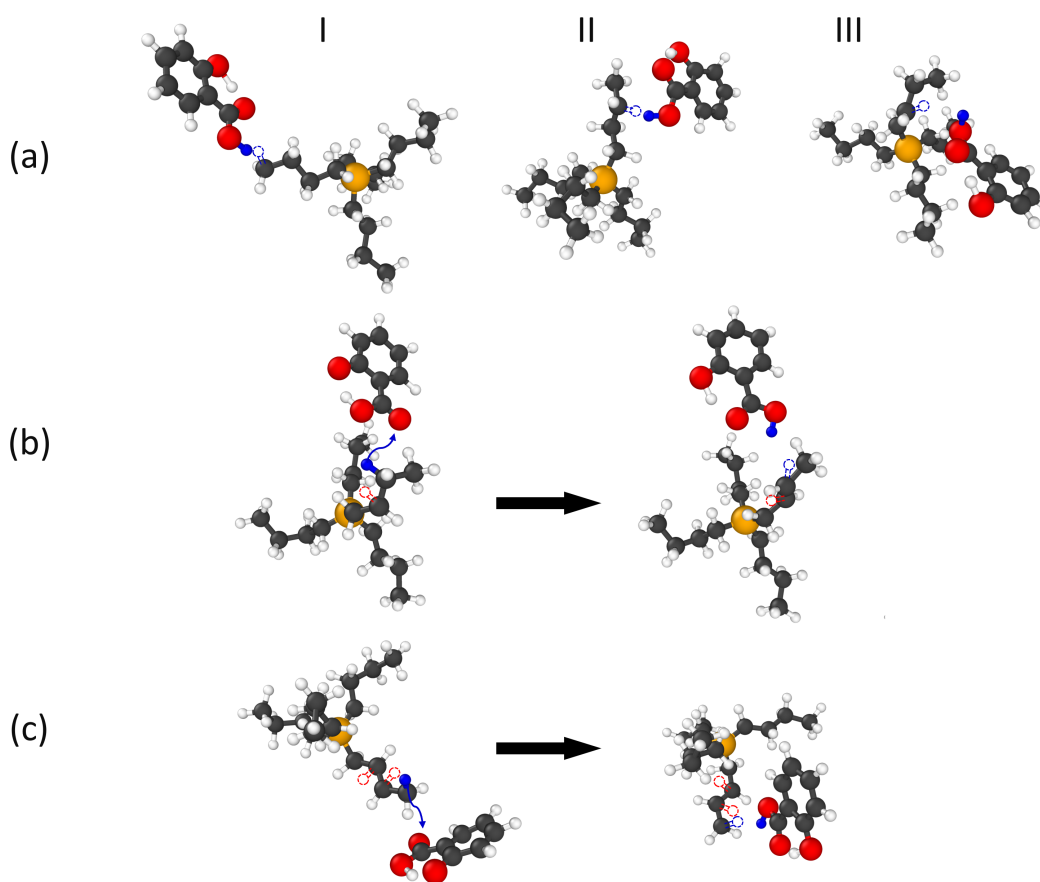
15

Figure 7: Snapshots show the most frequent reactions observed for phosphonium salicylate in order of decreasing net occurrence: (a) 47, (b) 17, and (c) 8. The newly transferred proton is shown in blue, as a solid sphere on the anion and a dashed blue circle on the cation. The hydrogen atoms that were removed from the cation in previous reactions are shown as dashed red circles. Note that (a) shows three configurations (labeled I, II, and III) after the proton-transfer from different carbon atoms in the cation alkyl chain to the salicylate anion.

stability of these phosphonium-based ILs.

To explore the effect of proton-transfer reactions on thermal stability, the number of reactions with a protonated anion as a product was calculated and found to be 620 for salicylate and 2409 for benzoate. Then, the contribution of each oxygen atom in receiving protons was quantified as the fraction of total protons received by each oxygen atom, as shown in Fig. 9(a). In benzoate, the contribution of the two oxygen atoms (O1 and O2) in proton-exchange reactions is nearly equal, which is reasonable considering the symmetry

of the benzoate structure. However, O2 in salicylate has a significantly lower contribution (only 4%) to proton-exchange reactions than the O1 (91%). The hydroxyl group (O3-H) pointing to O2 indicates the presence of a hydrogen bond (H-bond) between O3 and O2. The results imply that the intramolecular H-bond hinders the ability of O2 to take part in reactions and, therefore, contributes to the lower reactivity of O2 in salicylate compared to O2 in benzoate.

The hydrogen bonding within the structure of salicylate likely affects its thermal stability and is reflected by the differences in the number of proton-transfer reactions occurred for O2. However, analysis indicates that proton-transfer reactions for O1, that is not affected by H-bonding, also differs for the two anions. Specifically, it was found that there is a significant difference between the number of reactions in two anions: 564 for salicylate and 1229 for benzoate. This suggests there are factors contributing to the number of thermal decomposition reactions other than H-bonding. To understand why there are far fewer thermal decomposition reactions involving O1 in phosphonium salicylate than in phosphonium benzoate, the charge distribution on the anions was calculated. Fig. 9(b) shows the charge on each atom, averaged over 100 anions and 250 ns at 300 K. The charge of the O1 in salicylate (-0.65) is close to the charge of O1 in benzoate (-0.66). This is also observed during heating (see Fig. S3), so the charge distribution cannot explain the lower reactivity of O1 in salicylate compared to benzoate.

Another possible contributing factor is the effect of the salicylate hydroxyl group on the distance between the anions and cations. Radial distribution functions (RDFs) were used to quantify the distance between cations and anions, averaged over the last 250 ps of the equilibration simulations. Fig. 10(a) shows the RDF for the distance between all carbon atoms in the cation and the oxygen atoms in the anion ($\text{RDF}_{\text{O}_{\text{anion}}\text{-C}_{\text{cation}}}$). As shown in this figure, the position of the first peak is at 3.1 Å for both ILs. However, the peak for phosphonium benzoate is higher than that for phosphonium salicylate, indicating more benzoate cations are close to the alkyl chain of the phosphonium compared to the salicylate. The higher

population of carbon atoms around the oxygen atoms increases the possibility of proton-transfer between anion and cation. Another difference is the relative distance between the oxygen and phosphorous atoms in the two IL systems. The peak for the $\text{RDF}_{\text{O}_{\text{anion}}\text{-P}_{\text{cation}}}$, in Fig. 10(b), is higher and shifted slightly to the left for benzoate compared to salicylate. This suggests it is easier for the benzoate to approach the core of the phosphonium cation. The stronger P-O interactions (higher peak of $\text{RDF}_{\text{O}_{\text{anion}}\text{-P}_{\text{cation}}}$) in phosphonium benzoate compared to phosphonium salicylate can explain why there are more fragments in phosphonium benzoate, i.e., these fragments form through bonding between phosphorous and oxygen atoms (Fig. 8). This effect was not observed in phosphonium salicylate. All of the above observations suggest the hydroxyl groups in salicylate make this anion thermally more stable by hindering the chemical reactions for O2 as well as decreasing the strength of interactions between the anion and alkyl chains.
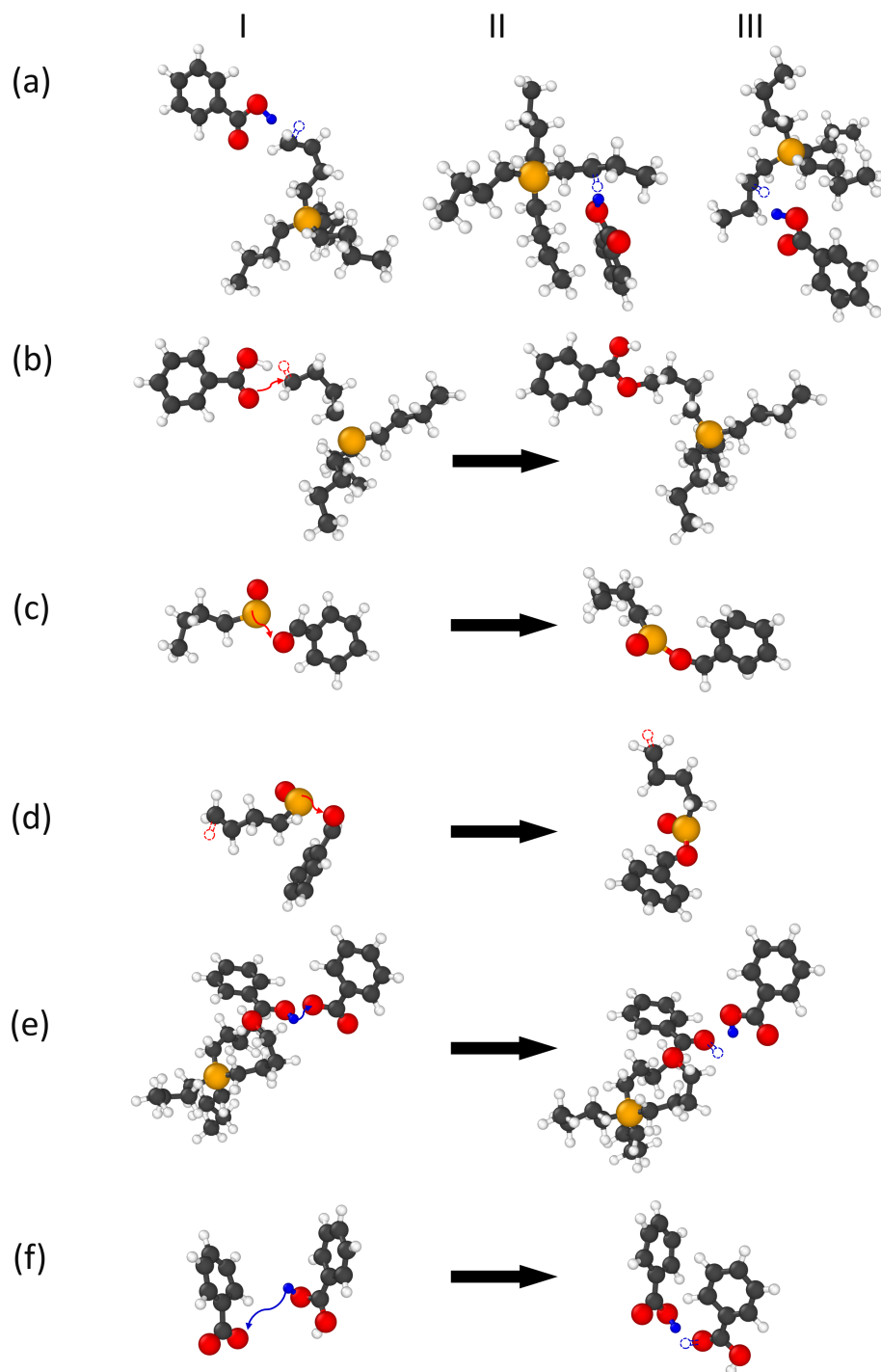
Figure 8: Snapshots show the most frequent reactions observed for phosphonium benzoate in order of decreasing net occurrence: (a) 52, (b) 19, (c) 16, (d) 16, (e) 12, and (f) 10. The newly transferred proton is shown in blue, as a solid sphere on the anion and a dashed blue circle on the cation. The hydrogen atoms that were removed from the cation in previous reactions are shown as dashed red circles. Note that (a) shows the three configurations after the proton-transfer from different carbon atoms in the alkyl chains of cation to the benzoate anion.
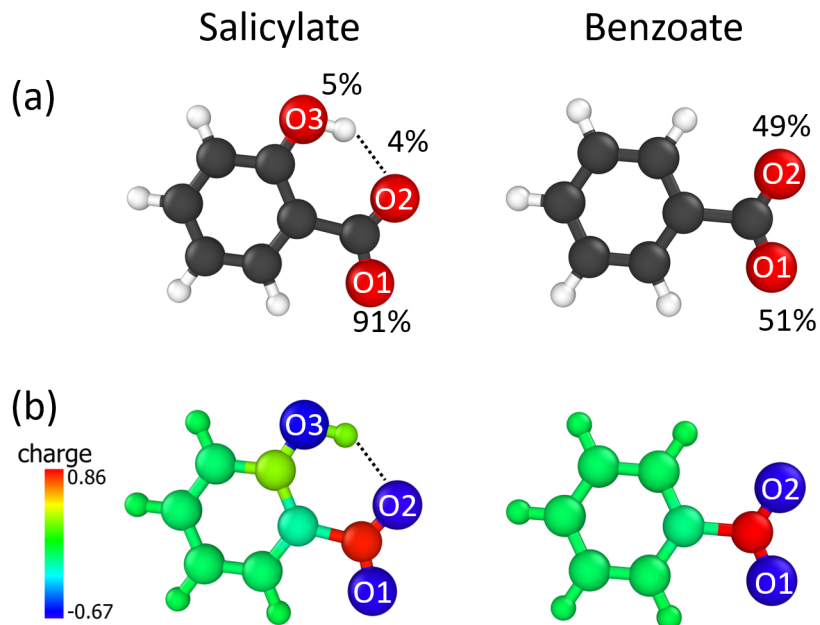
Figure 9: Atomic structures of salicylate (left) and benzoate (right). The difference between the two anions is the presence of the hydroxyl group next to the carboxylate in salicylate. (a) The contribution of each oxygen atom in receiving protons is indicated as percentage next to the atom. The percentages show that the participation of O2 in proton-transfer reaction is significantly lower in salicylate compared to benzoate. This can be explained by hydrogen bonding between O3 and O2 in the salicylate. (b) Color maps showing the average charge of atoms during the last 250 ps of equilibration simulation. The charge differences for oxygen atoms are very small and can not explain the different behavior of the two anions in proton-transfer reactions.
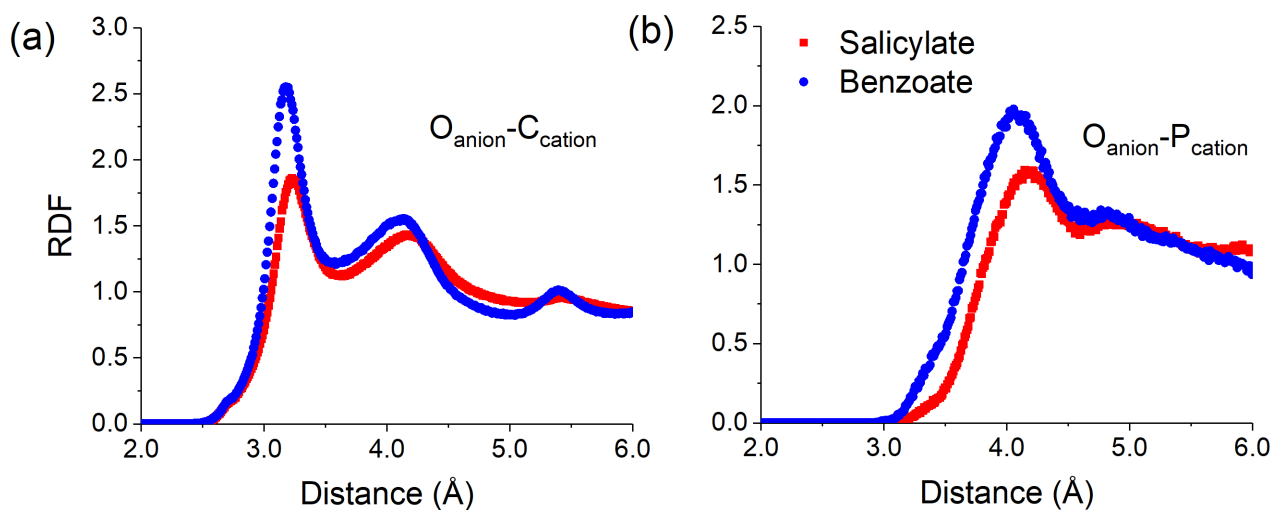
Figure 10: Radial distribution functions for (a) the distance between all carbon atoms in the cation and the central oxygen atoms in the anion (O_{anion}-C_{cation}) and (b) between the oxygen atoms in the anions and phosphorous atoms in the cations (O_{anion}-P_{cation}). The RDFs were calculated over 250ps at the end of the equilibration simulation and show the relative positions of atoms in the anions and cations for the two ILs. The higher O_{anion}-C_{cation} RDF peak in benzoate than salicylate in (a) indicates a stronger interaction between benzoate and phosphonium and suggests that benzoate anions can get closer to carbon atoms in the phosphonium cations. This can explain the easier proton-transfer from alkyl chains to benzoate compared to salicylate. The higher O_{anion}-P_{cation} RDF peak in (b) shows that approaching the core of the phosphonium cation is easier for benzoate than salicylate, which can explain more dissociated species observed in phosphonium benzoate.

Conclusions

Reactive MD simulations and thermogravimetric analysis were used to explore the thermal decomposition mechanisms of phosphonium salicylate and phosphonium benzoate. Thermogravimetric degradation experiments showed that both phosphonium salicylate and phosphonium benzoate had high thermal stability with decomposition temperatures above 600 K, making them suitable for high-temperature applications. The decomposition temperature increased for both phosphonium salicylate and phosphonium benzoate with increasing heating rate. Experiments at different heating rates indicated that the decomposition temperatures of phosphonium salicylate and phosphonium benzoate were comparable. However, isothermal decomposition tests showed that phosphonium benzoate was less stable than phosphonium salicylate, especially at high temperatures.

Reactive MD simulations were carried out to identify the mechanisms underlying thermal stability of these ionic liquids. The results showed there was no statistically significant effect of the cation chain length, whereas the anion played a more important role. The average onset temperature of thermal decomposition for phosphonium salicylate was significantly higher (668 K) than that for benzoate (486 K). This was consistent with the trends observed in the isothermal decomposition tests.

From the simulations, chemical reactions were identified through the connectivity of atoms and the composition of chemical species. The reaction steps were classified into three categories: proton-transfer, association, and dissociation, for both phosphonium salicylate and phosphonium benzoate. The number of distinct chemical reactions and occurrences of the different reaction pathways in each category were found to be higher for phosphonium benzoate than phosphonium salicylate, and this difference was correlated to the lower thermal stability of the benzoate. Importantly, all of the reaction pathways began with proton-transfer for both ILs.

Multiple possible reasons for the lower thermal stability of phosphonium benzoate were investigated. First, the presence of the hydroxyl group on the salicylate was shown to hinder

22

the ability of O2 oxygen atoms to take part in the proton-transfer reactions. Analysis showed that the two oxygen atoms in benzoate contributed almost equally to proton-transfer but that, in salicylate, the O2 (adjacent to the hydroxyl) had a significantly lower contribution than the O1. The total number of proton-transfer reactions for O1 that did not involve in H-bond in benzoate was found more than twice that in salicylate. The higher density of carbon atoms around the oxygen atoms (higher O_{anion}-C_{cation} RDF peak) explained the increased the possibility of proton-transfer between anion and cation in phosphonium benzoate. Lastly, the peak of the distribution of distances between oxygen in the anion and carbon or phosphorous in the cation was found to be higher for phosphonium benzoate than phosphonium salicylate. This indicates it is easier for the benzoate to approach the core of the phosphonium cation, therefore facilitating the interactions that lead to decomposition.

Overall, this study demonstrated that even a relatively small chemical change in an anion, e.g., the presence of a hydroxyl group in salicylate and not in benzoate, can significantly affect the thermal stability of phosphonium-based ILs. The mechanism underlying this affect was shown to be the effect of the anion on the proton-transfer reaction that was the first step of all subsequent decomposition pathways. Although these findings were demonstrated here for phosphonium benzoate compared to phosphonium salicylate, the results may be more generally relevant and suggest avenues for optimizing thermal decomposition behavior for ILs through molecular design.

Acknowledgement

References

(1) Sowmiah, S.; Srinivasadesikan, V.; Tseng, M.-C.; Chu, Y.-H. On the chemical stabilities of ionic liquids. *Molecules* **2009**, *14*, 3780–3813.

(2) Goossens, K.; Lava, K.; Bielawski, C. W.; Binnemans, K. Ionic liquid crystals: versatile materials. *Chem. Rev.* **2016**, *116*, 4643–4807.

(3) Krannich, M.; Heym, F.; Jess, A. Characterization of six hygroscopic ionic liquids with regard to their suitability for gas dehydration: density, viscosity, thermal and oxidative stability, vapor pressure, diffusion coefficient, and activity coefficient of water. *J. Chem. Eng. Data* **2016**, *61*, 1162–1176.

(4) Ahrenberg, M.; Beck, M.; Neise, C.; Keßler, O.; Kragl, U.; Verevkin, S. P.; Schick, C. Vapor pressure of ionic liquids at low temperatures from AC-chip-calorimetry. *Phys. Chem. Chem. Phys.* **2016**, *18*, 21381–21390.

(5) Eftekhari, A.; Liu, Y.; Chen, P. Different roles of ionic liquids in lithium batteries. *J. Power Sources* **2016**, *334*, 221–239.

(6) Griffin, P. J.; Freyer, J. L.; Han, N.; Geller, N.; Yin, X.; Gheewala, C. D.; Lambert, T. H.; Campos, L. M.; Winey, K. I. Ion transport in cyclopropenium-based polymerized ionic liquids. *Macromol.* **2018**, *51*, 1681–1687.

(7) Rabideau, B. D.; West, K. N.; Davis, J. H. Making good on a promise: ionic liquids with genuinely high degrees of thermal stability. *Chem. Commun.* **2018**, *54*, 5019–5031.

(8) Rybińska-Fryca, A.; Mikolajczyk, A.; Łuczak, J.; Paszkiewicz-Gawron, M.; Paszkiewicz, M.; Zaleska-Medynska, A.; Puzyn, T. How thermal stability of ionic liquids leads to more efficient TiO2-based nanophotocatalysts: Theoretical and experimental studies. *J. Colloid Interface Sci.* **2020**, *572*, 396–407.

(9) Kunz, W.; Häckl, K. The hype with ionic liquids as solvents. *Chem. Phys. Lett.* **2016**, *661*, 6–12.

(10) Yoo, C. G.; Pu, Y.; Ragauskas, A. J. Ionic liquids: Promising green solvents for lignocellulosic biomass utilization. *Curr. Opin. Green Sustain.* **2017**, *5*, 5–11.

(11) Karodia, N.; Guise, S.; Newlands, C.; Andersen, J.-A. Clean catalysis with ionic solvents—phosphonium tosylates for hydroformylation. *Chem. Commun.* **1998**, 2341–2342.

(12) Earle, M. J.; Seddon, K. R. Ionic liquids. Green solvents for the future. *Pure Appl. Chem.* **2000**, *72*, 1391–1398.

(13) Long, T. E.; Ramirez, S. M.; Heflin, R.; Gibson, H. W.; Madsen, L. A.; Leo, D. J.; Goulbourne, N.; Wilkes, G. L.; Winey, K. I.; Elabd, Y. A. et al. *Ionic Liquids for Advanced Materials*; 2008.

(14) Roper, A. R. Ionic Liquid Crystal Polymers for Display Devices: A Study of Mesogenic Diallylamine-Terminated Polymers. Ph.D. thesis, University of York, 2016.

(15) Diaz, M.; Ortiz, A.; Ortiz, I. Progress in the use of ionic liquids as electrolyte membranes in fuel cells. *J. Membr. Sci.* **2014**, *469*, 379–396.

(16) Watanabe, M.; Thomas, M. L.; Zhang, S.; Ueno, K.; Yasuda, T.; Dokko, K. Application of ionic liquids to energy storage and conversion materials and devices. *Chem. Rev.* **2017**, *117*, 7190–7239.

(17) Balducci, A. Ionic liquids in lithium-ion batteries. *Ionic Liq. II* **2017**, 1–27.

(18) Sakaebe, H.; Matsumoto, H.; Tatsumi, K. Application of room temperature ionic liquids to Li batteries. *Electrochim. Acta* **2007**, *53*, 1048–1054.

(19) Mittenthal, M. S.; Flowers, B. S.; Bara, J. E.; Whitley, J. W.; Spear, S. K.; Roveda, J. D.; Wallace, D. A.; Shannon, M. S.; Holler, R.; Martens, R. et al. Ionic

polyimides: hybrid polymer architectures and composites with ionic liquids for advanced gas separation membranes. *Ind. Eng. Chem. Res.* **2017**, *56*, 5055–5069.

(20) Shang, D.; Liu, X.; Bai, L.; Zeng, S.; Xu, Q.; Gao, H.; Zhang, X. Ionic liquids in gas separation processing. *Curr. Opin. Green Sustain.* **2017**, *5*, 74–81.

(21) Zhou, Y.; Qu, J. Ionic liquids as lubricant additives: a review. *ACS Appl. Mater. Interfaces* **2017**, *9*, 3209–3222.

(22) Amiril, S.; Rahim, E.; Syahrullail, S. A review on ionic liquids as sustainable lubricants in manufacturing and engineering: Recent research, performance, and applications. *J. Cleaner Prod.* **2017**, *168*, 1571–1589.

(23) Scott, M. P.; Rahman, M.; Brazel, C. S. Application of ionic liquids as low-volatility plasticizers for PMMA. *Eur. Polym. J.* **2003**, *39*, 1947–1953.

(24) Patil, R. A.; Talebi, M.; Xu, C.; Bhawal, S. S.; Armstrong, D. W. Synthesis of thermally stable geminal dicationic ionic liquids and related ionic compounds: an examination of physicochemical properties by structural modification. *Chem. Mater.* **2016**, *28*, 4315–4323.

(25) Bermúdez, M.-D.; Jiménez, A.-E.; Sanes, J.; Carrión, F.-J. Ionic liquids as advanced lubricant fluids. *Molecules* **2009**, *14*, 2888–2908.

(26) Qiao, Y.; Ma, W.; Theyssen, N.; Chen, C.; Hou, Z. Temperature-responsive ionic liquids: fundamental behaviors and catalytic applications. *Chem. Rev.* **2017**, *117*, 6881–6928.

(27) Ngo, H. L.; LeCompte, K.; Hargens, L.; McEwen, A. B. Thermal properties of imidazolium ionic liquids. *Thermochim. Acta* **2000**, *357*, 97–102.

(28) Bonhote, P.; Dias, A.-P.; Papageorgiou, N.; Kalyanasundaram, K.; Grätzel, M. Hydrophobic, highly conductive ambient-temperature molten salts. *Inorg. Chem.* **1996**, *35*, 1168–1178.

(29) Kosmulski, M.; Gustafsson, J.; Rosenholm, J. B. Thermal stability of low temperature ionic liquids revisited. *Thermochim. Acta* **2004**, *412*, 47–53.

(30) Anderson, J. L.; Armstrong, D. W. High-stability ionic liquids. A new class of stationary phases for gas chromatography. *Anal. Chem.* **2003**, *75*, 4851–4858.

(31) Meine, N.; Benedito, F.; Rinaldi, R. Thermal stability of ionic liquids assessed by potentiometric titration. *Green Chem.* **2010**, *12*, 1711–1714.

(32) Villanueva, M.; Coronas, A.; García, J.; Salgado, J. Thermal stability of ionic liquids for their application as new absorbents. *Ind. Eng. Chem. Res.* **2013**, *52*, 15718–15727.

(33) Cassity, C. G.; Mirjafari, A.; Mobarrez, N.; Strickland, K. J.; O'Brien, R. A.; Davis, J. H. Ionic liquids of superior thermal stability. *Chem. Commun.* **2013**, *49*, 7590–7592.

(34) Wang, W.; Ma, X.; Grimes, S.; Cai, H.; Zhang, M. Study on the absorbability, regeneration characteristics and thermal stability of ionic liquids for VOCs removal. *Chem. Eng. J.* **2017**, *328*, 353–359.

(35) Xu, C.; Cheng, Z. Thermal Stability of Ionic Liquids: Current Status and Prospects for Future Development. *Processes* **2021**, *9*, 337.

(36) Sepehri, B. A review on created QSPR models for predicting ionic liquids properties and their reliability from chemometric point of view. *J. Mol. Liq.* **2020**, *297*, 112013.

(37) Rahman, M. H.; Khajeh, A.; Panwar, P.; Patel, M.; Martini, A.; Menezes, P. L. Recent progress on phosphonium-based room temperature ionic liquids: Synthesis, properties, tribological performances and applications. *Tribol. Int.* **2022**, *167*, 107331.

(38) Plechkova, N. V.; Seddon, K. R. Applications of ionic liquids in the chemical industry. *Chem. Soc. Rev.* **2008**, *37*, 123–150.

(39) Barbosa, M. S.; Freire, C. C.; Souza, R. L.; Cabrera-Padilla, R. Y.; Pereira, M. M.; Freire, M. G.; Lima, Á. S.; Soares, C. M. Effects of phosphonium-based ionic liquids on the lipase activity evaluated by experimental results and molecular docking. *Biotechnol. Prog.* **2019**, *35*, e2816.

(40) Ferreira, A. F.; Simões, P. N.; Ferreira, A. G. Quaternary phosphonium-based ionic liquids: Thermal stability and heat capacity of the liquid phase. *J. Chem. Thermodyn.* **2012**, *45*, 16–27.

(41) Battez, A. H.; Bartolomé, M.; Blanco, D.; Viesca, J.; Fernández-González, A.; González, R. Phosphonium cation-based ionic liquids as neat lubricants: Physico-chemical and tribological performance. *Tribol. Int.* **2016**, *95*, 118–131.

(42) Green, M. D.; Schreiner, C.; Long, T. E. Thermal, rheological, and ion-transport properties of phosphonium-based ionic liquids. *J. Phys. Chem. A* **2011**, *115*, 13829–13835.

(43) Del Sesto, R. E.; Corley, C.; Robertson, A.; Wilkes, J. S. Tetraalkylphosphonium-based ionic liquids. *J. Organomet. Chem.* **2005**, *690*, 2536–2542.

(44) Wang, Y.-L.; Shah, F. U.; Glavatskih, S.; Antzutkin, O. N.; Laaksonen, A. Atomistic insight into orthoborate-based ionic liquids: force field development and evaluation. *J. Phys. Chem. B* **2014**, *118*, 8711–8723.

(45) Maton, C.; De Vos, N.; Stevens, C. V. Ionic liquid thermal stabilities: decomposition mechanisms and analysis tools. *Chem. Soc. Rev.* **2013**, *42*, 5963–5977.

(46) Deferm, C.; Van den Bossche, A.; Luyten, J.; Oosterhof, H.; Fransaer, J.; Bin-

nemans, K. Thermal stability of trihexyl (tetradecyl) phosphonium chloride. *Phys. Chem. Chem. Phys.* **2018**, *20*, 2444–2456.

(47) Liu, Y.; Cheng, W.; Zhang, Y.; Sun, J.; Zhang, S. Controllable preparation of phosphonium-based polymeric ionic liquids as highly selective nanocatalysts for the chemical conversion of CO 2 with epoxides. *Green Chem.* **2017**, *19*, 2184–2193.

(48) Keating, M. Y.; Gao, F.; Ramsey, J. B. TGA-MS study of the decomposition of phosphorus-containing ionic liquids trihexyl (tetradecyl) phosphonium decanoate and trihexyltetradecylphosphonium bis [(trifluoromethyl) sulfonyl] amide. *J. Therm. Anal. Calorim.* **2011**, *106*, 207–211.

(49) Patil, R. A.; Talebi, M.; Berthod, A.; Armstrong, D. W. Dicationic ionic liquid thermal decomposition pathways. *Anal. Bioanal. Chem.* **2018**, *410*, 4645–4655.

(50) Uddin, M. N.; Basak, D.; Hopefl, R.; Minofar, B. Potential application of ionic liquids in pharmaceutical dosage forms for small molecule drug and vaccine delivery system. *J. Pharm. Pharm. Sci.* **2020**, *23*, 158–176.

(51) Jia, Y.-W.; Zhao, X.; Fu, T.; Li, D.-F.; Guo, Y.; Wang, X.-L.; Wang, Y.-Z. Synergy effect between quaternary phosphonium ionic liquid and ammonium polyphosphate toward flame retardant PLA with improved toughness. *Composites, Part B* **2020**, *197*, 108192.

(52) Golets, M.; Shimpi, M.; Wang, Y.-L.; Antzutkin, O.; Glavatskih, S.; Laaksonen, A. Understanding the thermal decomposition mechanism of a halogen-free chelated orthoborate-based ionic liquid: a combined computational and experimental study. *Phys. Chem. Chem. Phys.* **2016**, *18*, 22458–22466.

(53) Cecchini, M. M.; Steinkoenig, J.; Reale, S.; Barner, L.; Yuan, J.; Goldmann, A. S.; De Angelis, F.; Barner-Kowollik, C. Universal mass spectrometric analysis of poly (ionic liquid) s. *Chem. Sci.* **2016**, *7*, 4912–4921.

(54) Liu, T.; Panwar, P.; Khajeh, A.; Rahman, M. H.; Menezes, P. L.; Martini, A. Review of Molecular Dynamics Simulations of Phosphonium Ionic Liquidss. *Tribol. Lett.* **Submitted**,

(55) Kroon, M. C.; Buijs, W.; Peters, C. J.; Witkamp, G.-J. Quantum chemical aided prediction of the thermal decomposition mechanisms and temperatures of ionic liquids. *Thermochim. Acta* **2007**, *465*, 40–47.

(56) Cassity, C. A.; Siu, B.; Soltani, M.; McGeehee, J. L.; Strickland, K. J.; Vo, M.; Salter, E. A.; Stenson, A. C.; Wierzbicki, A.; West, K. N. et al. The effect of structural modifications on the thermal stability, melting points and ion interactions for a series of tetraaryl-phosphonium-based mesothermal ionic liquids. *Phys. Chem. Chem. Phys.* **2017**, *19*, 31560–31571.

(57) Boudewijns, T.; Piccinini, M.; Degraeve, P.; Liebens, A.; De Vos, D. Pathway to vinyl chloride production via dehydrochlorination of 1, 2-dichloroethane in ionic liquid media. *ACS Catal.* **2015**, *5*, 4043–4047.

(58) Senftle, T. P.; Hong, S.; Islam, M. M.; Kylasa, S. B.; Zheng, Y.; Shin, Y. K.; Junkermeier, C.; Engel-Herbert, R.; Janik, M. J.; Aktulga, H. M. et al. The ReaxFF reactive force-field: development, applications and future directions. *npj Comput. Mater.* **2016**, *2*, 15011.

(59) Martini, A.; Eder, S. J.; Dörr, N. Tribochemistry: A review of reactive molecular dynamics simulations. *Lubricants* **2020**, *8*, 44.

(60) Van Duin, A. C.; Dasgupta, S.; Lorant, F.; Goddard, W. A. ReaxFF: a reactive force field for hydrocarbons. *J. Phys. Chem. A* **2001**, *105*, 9396–9409.

(61) Chenoweth, K.; Cheung, S.; Van Duin, A. C.; Goddard, W. A.; Kober, E. M. Simulations on the thermal decomposition of a poly (dimethylsiloxane) polymer using the ReaxFF reactive force field. *J. Am. Chem. Soc.* **2005**, *127*, 7192–7202.

(62) Han, S.; Li, X.; Guo, L.; Sun, H.; Zheng, M.; Ge, W. Refining fuel composition of RP-3 chemical surrogate models by reactive molecular dynamics and machine learning. *Energy & Fuels* **2020**, *34*, 11381–11394.

(63) Gao, M.; Li, X.; Guo, L. Pyrolysis simulations of Fugu coal by large-scale ReaxFF molecular dynamics. *Fuel Process. Technol.* **2018**, *178*, 197–205.

(64) Xin, L.; Liu, C.; Liu, Y.; Huo, E.; Li, Q.; Wang, X.; Cheng, Q. Thermal decomposition mechanism of some hydrocarbons by ReaxFF-based molecular dynamics and density functional theory study. *Fuel* **2020**, *275*, 117885.

(65) Huo, E.; Liu, C.; Xu, X.; Dang, C. A ReaxFF-based molecular dynamics study of the pyrolysis mechanism of HFO-1336mzz(Z). *International Journal of Refrigeration* **2017**, *83*, 118–130.

(66) Cao, Y.; Liu, C.; Zhang, H.; Xu, X.; Li, Q. Thermal decomposition of HFO-1234yf through ReaxFF molecular dynamics simulation. *Appl. Therm. Eng.* **2017**, *126*, 330–338.

(67) Liu, Y.; Hu, J.; Hou, H.; Wang, B. Development and application of a ReaxFF reactive force field for molecular dynamics of perfluorinatedketones thermal decomposition. *Chem. Phys.* **2020**, *538*, 110888.

(68) Lyu, R.; Huang, Z.; Deng, H.; Wei, Y.; Mou, C.; Wang, L. Anatomies for the thermal decomposition behavior and product rule of 5,5-dinitro-2H,2H-3,3-bi-1,2,4-triazole. *RSC Adv.* **2021**, *11*, 40182–40192.

(69) Lan, G.; Li, J.; Zhang, G.; Ruan, J.; Lu, Z.; Jin, S.; Cao, D.; Wang, J. Thermal decomposition mechanism study of 3-nitro-1, 2, 4-triazol-5-one (NTO): Combined TG-FTIR-MS techniques and ReaxFF reactive molecular dynamics simulations. *Fuel* **2021**, *295*, 120655.

(70) Khajeh, A.; Bhuiyan, F. H.; Mogonye, J.-E.; Pesce-Rodriguez, R. A.; Berkebile, S.; Martini, A. Thermal Decomposition of Tricresyl Phosphate on Ferrous Surfaces. *J. Phys. Chem. C* **2021**, *125*, 5076–5087.

(71) Ewen, J. P.; Latorre, C. A.; Gattinoni, C.; Khajeh, A.; Moore, J. D.; Remias, J. E.; Martini, A.; Dini, D. Substituent Effects on the Thermal Decomposition of Phosphate Esters on Ferrous Surfaces. *J. Phys. Chem. C* **2020**, *124*, 9852–9865.

(72) Zhang, B.; van Duin, A. C.; Johnson, J. K. Development of a ReaxFF reactive force field for tetrabutylphosphonium glycinate/CO2 mixtures. *J. Phys. Chem. B* **2014**, *118*, 12008–12016.

(73) Singhai, S. Application of the ReaxFF Molecular Simulation Method for Investigating Hypergolicity of Energetic Ionic Liquids. **2010**,

(74) Borodin, O.; Smith, G.; Bedrov, D.; Van Duin, A.; Gorecki, W.; Armand, M. Insight into Electrolyte Structure, Transport and Reduction Pathways from Molecular Dynamics Simulations. ECS Meeting Abstracts. 2010; p 202.

(75) Liu, Y.; Yu, P.; Wu, Y.; Yang, H.; Xie, M.; Huai, L.; Goddard III, W. A.; Cheng, T. The DFT-ReaxFF Hybrid Reactive Dynamics Method with Application to the Reductive Decomposition Reaction of the TFSI and DOL Electrolyte at a Lithium–Metal Anode Surface. *J. Phys. Chem. Lett.* **2021**, *12*, 1300–1306.

(76) Egorov, V. M.; Djigailo, D. I.; Momotenko, D. S.; Chernyshov, D. V.; Torocheshnikova, I. I.; Smirnova, S. V.; Pletnev, I. V. Task-specific ionic liquid trioctylmethylammonium salicylate as extraction solvent for transition metal ions. *Talanta* **2010**, *80*, 1177–1182.

(77) Reeves, C. J.; Kasar, A. K.; Menezes, P. L. Tribological performance of environmental friendly ionic liquids for high-temperature applications. *J. Cleaner Prod.* **2021**, *279*, 123666.

(78) ASTM E 2550-17, Standard Test Method for Thermal Stability by Thermogravimetre, ASTM International. *ASTM International, West Conshohocken, PA* **2018**,

(79) Wooster, T. J.; Johanson, K. M.; Fraser, K. J.; MacFarlane, D. R.; Scott, J. L. Thermal degradation of cyano containing ionic liquids. *Green Chem.* **2006**, *8*, 691–696.

(80) Salgado, J.; Parajó, J. J.; Fernández, J.; Villanueva, M. Long-term thermal stability of some 1-butyl-1-methylpyrrolidinium ionic liquids. *J. Chem. Thermodyn.* **2014**, *74*, 51–57.

(81) Salgado, J.; Villanueva, M.; Parajó, J. J.; Fernández, J. Long-term thermal stability of five imidazolium ionic liquids. *J. Chem. Thermodyn.* **2013**, *65*, 184–190.

(82) Adamová, G.; Gardas, R. L.; Rebelo, L. P. N.; Robertson, A. J.; Seddon, K. R. Alkyltrioctylphosphonium chloride ionic liquids: synthesis and physicochemical properties. *Dalton Trans.* **2011**, *40*, 12750–12764.

(83) Sydow, M.; Owsianiak, M.; Framski, G.; Woźniak-Karczewska, M.; Piotrowska-Cyplik, A.; Ławniczak, Ł.; Szulc, A.; Zgoła-Grześkowiak, A.; Heipieper, H. J.; Chrzanowski, Ł. Biodiversity of soil bacteria exposed to sub-lethal concentrations of phosphonium-based ionic liquids: Effects of toxicity and biodegradation. *Ecotoxicol. Environ. Saf.* **2018**, *147*, 157–164.

(84) Parajó, J. J.; Macário, I. P.; De Gaetano, Y.; Dupont, L.; Salgado, J.; Pereira, J. L.; Gonçalves, F. J.; Mohamadou, A.; Ventura, S. P. Glycine-betaine-derived ionic liquids: Synthesis, characterization and ecotoxicological evaluation. *Ecotoxicol. Environ. Saf.* **2019**, *184*, 109580.

(85) Evans, D. J.; Holian, B. L. The Nose–Hoover thermostat. *The Journal of Chem. Phys.* **1985**, *83*, 4069–4074.

(86) Plimpton, S. Fast parallel algorithms for short-range molecular dynamics. *J. Comput. Phys.* **1995**, *117*, 1–19.

(87) Stukowski, A. Visualization and analysis of atomistic simulation data with OVITO– the Open Visualization Tool. *Modell. Simul. Mater. Sci. Eng.* **2009**, *18*, 015012.

(88) Thermal Stability. Glossary 2021. *Available from: https://www.netzsch-thermal-analysis.com/us/commercial-testing/glossary/thermal-stability/*

(89) Khajeh, A.; Krim, J.; Martini, A. Synergistic effect of nanodiamonds on the adsorption of tricresyl phosphate on iron oxide surfaces. *Appl. Phys. Lett.* **2019**, *114*, 171602.

(90) Zhang, L.; Duin, A. C. v.; Zybin, S. V.; Goddard Iii, W. A. Thermal decomposition of hydrazines from reactive dynamics using the ReaxFF reactive force field. *J. Phys. Chem. B* **2009**, *113*, 10770–10778.

(91) Stein, O.; Lin, Z.; Zhigilei, L. V.; Asscher, M. Selective ablation of Xe from silicon surfaces: molecular dynamics simulations and experimental laser patterning. *J. Phys. Chem. A* **2011**, *115*, 6250–6259.

(92) Schittkowski, J.; Buesen, D.; Toelle, K.; Muhler, M. The Temperature-Programmed Desorption of H 2 from Cu/ZrO 2. *Catal. Lett.* **2016**, *146*, 1011–1017.

(93) Cao, Y.; Mu, T. Comprehensive investigation on the thermal stability of 66 ionic liquids by thermogravimetric analysis. *Ind. Eng. Chem. Res.* **2014**, *53*, 8651–8664.

(94) Brauer, U. G.; Andreah, T.; Miller, K. M. The effect of counteranion on the physico-chemical and thermal properties of 4-methyl-1-propyl-1, 2, 4-triazolium ionic liquids. *J. Mol. Liq.* **2015**, *210*, 286–292.

(95) Chatel, G.; Pereira, J. F.; Debbeti, V.; Wang, H.; Rogers, R. D. Mixing ionic liquids– "simple mixtures" or "double salts"? *Green Chem.* **2014**, *16*, 2051–2083.

(96) Gorantla, K. R.; Mallik, B. S. Reaction Mechanism and Free Energy Barriers for the Chemisorption of CO2 by Ionic Entities. *J. Phys. Chem. A* **2020**, *124*, 836–848.

(97) Mercy, M.; de Leeuw, N. H.; Bell, R. G. Mechanisms of CO2 capture in ionic liquids: a computational perspective. *Faraday Discuss.* **2016**, *192*, 479–492.

(98) Laszlo, K. J.; Bush, M. F. Interpreting the collision cross sections of native-like protein ions: insights from cation-to-anion proton-transfer reactions. *Anal. Chem.* **2017**, *89*, 7607–7614.

(99) Gadzuk-Shea, M. M.; Bush, M. F. Effects of charge state on the structures of serum albumin ions in the gas phase: insights from cation-to-anion proton-transfer reactions, ion mobility, and mass spectrometry. *J. Phys. Chem. B* **2018**, *122*, 9947–9955.

(100) Carlin, C. M.; Gordon, M. S. Ab initio investigation of cation proton affinity and proton transfer energy for energetic ionic liquids. *J. Phys. Chem. A* **2016**, *120*, 6059–6063.

(101) Gao, H.; Zhang, Y.; Wang, H.-J.; Liu, J.; Chen, J. Theoretical study on the structure and cation- anion interaction of amino acid cation based amino acid ionic liquid $[Pro]^+[NO_3]^-$. *J. Phys. Chem. A* **2010**, *114*, 10243–10252.

TOC Graphic